HHS Public Access

Author manuscript

Nature. Author manuscript; available in PMC 2013 April 11.

Published in final edited form as:

Nature. 2012 October 11; 490(7419): 283–287. doi:10.1038/nature11398.

HIV-infected T cells are migratory vehicles for viral dissemination

Thomas T. Murooka[1], **Maud Deruaz**[1], **Francesco Marangoni**[1], **Vladimir D. Vrbanac**[1], **Edward Seung**[1], **Ulrich H. von Andrian**[2], **Andrew M. Tager**[1], **Andrew D. Luster**[1], and **Thorsten R. Mempel**[1,*]

[1]The Center for Immunology and Inflammatory Diseases, Massachusetts General Hospital, Harvard Medical School, Boston, MA

[2]Immune Disease Institute and Department of Microbiology and Immunology, Harvard Medical School, Boston, USA

Abstract

After host entry through mucosal surfaces, HIV-1 disseminates to lymphoid tissues to establish a generalized infection of the immune system. The mechanisms by which this virus spreads among permissive target cells locally during early stages of transmission, and systemically during subsequent dissemination are not known[1]. *In vitro* studies suggest that formation of virological synapses (VSs) during stable contacts between infected and uninfected T cells greatly increases the efficiency of viral transfer[2]. It is unclear, however, if T cell contacts are sufficiently stable *in vivo* to allow for functional synapse formation under the conditions of perpetual cell motility in epithelial[3] and lymphoid tissues[4]. Here, using multiphoton intravital microscopy (MP-IVM), we examined the dynamic behavior of HIV-infected T cells in lymph nodes (LNs) of humanized mice. We found that most productively infected T cells migrated robustly, resulting in their even distribution throughout the LN cortex. A subset of infected cells formed multinucleated syncytia through HIV envelope (Env)-dependent cell fusion. Both uncoordinated motility of syncytia as well as adhesion to $CD4^+$ LN cells led to the formation of long membrane tethers, increasing cell lengths to up to 10 times that of migrating uninfected T cells. Blocking the egress of migratory T cells from LNs into efferent lymph, and thus interrupting T cell recirculation, limited HIV dissemination and strongly reduced plasma viremia. Thus, we have found that HIV-infected T cells are motile, form syncytia, and establish tethering interactions that may facilitate cell-to-cell transmission through VSs. While their migration in LNs spreads infection locally, T cell recirculation through tissues is important for efficient systemic viral spread, suggesting new molecular targets to antagonize HIV infection.

*Correspondence should be addressed to: T.R.M. (tmempel@mgh.harvard.edu).

Supplementary Information is linked to the online version of the paper at www.nature.com/nature.

Author contributions T.T.M., M.D. and T.R.M. performed all experiments. F.M. developed software for data analysis. E.S. and V.V. generated humanized mice. A.M.T., A.D.L. and U.H.v.A contributed to the overall study design. T.T.M. and T.R.M. designed the experiments and wrote the manuscript.

Author information Reprints and permissions information is available at www.nature.com/reprints. The authors declare no competing financial interests.

Keywords

Human Immunodeficiency Virus (HIV)-1; Cell Migration; Lymph Node (LN); Multiphoton Intravital Microscopy (MP-IVM); Humanized Mice; T cell Trafficking

In HIV infection, lymph nodes are important sites of viral replication, where the high local density of $CD4^+$ T cells and other target cells may favor cell contact-mediated viral spread. Since infection of BLT (Bone marrow/Liver/Thymus) humanized mice[5] replicates many hallmarks of infection in humans[6–8], we utilized this small animal model (Supplementary Fig. 1a) and intravital microscopy to investigate the dynamic behavior of HIV-infected T cells in the stromal environment of LNs.

We first sought to validate this mouse model for studying the effects of HIV infection on T cell migration. The presence of both naïve and memory human $CD4^+$ and $CD8^+$ T cells in secondary lymphoid organs (SLOs) of BLT mice demonstrates their general capacity to home to these sites (Fig. 1a). To determine the efficiency of this trafficking process we infused BLT mice with mixtures of isogenic $CD4^+$ human T cells and murine $CD4^+$ T cells from OT-II TCR transgenic mice. Over the course of 18 hours, human T cells were half as efficient as murine cells at entering peripheral LNs, while their accumulation in mesenteric LNs was equivalent (Fig. 1b). Thus, the interspecies molecular interactions between selectins, chemokine receptors, and integrins on human T cells with their ligands expressed on murine LN high endothelial venules[9] are collectively functional, albeit at a slightly reduced level.

Upon entering LNs, T cell migration is guided by their sensing of chemokines[10] and interactions with the paracortical fibroblastic reticulum[11], which is well preserved in BLT mice (Supplementary Fig. 1b). We compared the migration of human and murine T cells in BLT LNs by MP-IVM. Intravenously infused human and murine cells distributed similarly in the LN cortex, were indistinguishable in various aspects of motility (Fig. 1c–e, Supplementary Fig. 1c–e and Video 1), and in this regard each resembled murine T cells in fully murine LNs[4]. We concluded that human T cell homing to LNs was efficient and their migration within LNs of BLT mice was, using mouse T cells as reference, normal, allowing us to study the impact of HIV infection on this basic process.

In order to seed LNs with HIV we injected BLT mice in the footpad with GFP-expressing, CCR5-using HIV (called ‘HIV-GFP’ here), which we derived by replacing the V3 loop region of *env* in the originally CXCR4-tropic NL4-3-IRES-GFP[12] with that of HIV BaL (Supplementary Fig. 2a, b). Subcutaneous infection reliably produced high levels of plasma viremia (Fig. 2a) and systemic infection (Supplementary Fig. 2c). However, between two and six days after footpad infection, we detected GFP^+ cells only in the ipsilateral popliteal, but not remote LNs, indicating that the infection was initially contained in the primary draining LNs (Fig. 2b, Supplementary Fig. 2e). The vast majority of these infected cells were resting (SSC^{low}), antigen-experienced ($CD45RO^+$) T cells with variable expression of CCR7. By day 2 some loss of CD4 cell surface expression was apparent[13], but this was much more pronounced at day 6, when cells had also downregulated MHC I. (Supplementary Fig. 2e).

To investigate the localization of HIV-infected T cells in LNs early after footpad infection, we analyzed draining LNs by MP-IVM two days after virus inoculation. At this time, GFP^+ cells were evenly distributed up to several hundred μm away from the subcapsular sinus (SCS), implying that lymph-borne HIV arriving in the LN SCS has efficient means of infiltrating the LN cortex (Fig. 2c). In time-lapse recordings it became apparent that GFP-expressing LN cells migrated at average 2D velocities of ~7 μm/min and were thus robustly motile, suggesting that their motility facilitated the local dissemination of HIV infection in LNs (Fig. 2d–f, Supplementary Video 2). Since the majority of infected T cells in early SIV-infection of macaques are resting memory T cells[14], and the majority of infected LN cells in our BLT mouse model resembled antigen-experienced T cells (Fig. 2b), we compared their motility to that of *in vitro*-generated, GFP-expressing, central memory-like $CD4^+$ human T cells ("Tcm") that express CD62L and CCR7 and migrate to LNs after adoptive transfer (Supplementary Fig. 3a–c). Compared to this reference population, the motility of HIV-infected LN cells was reduced (Fig. 2e, f, Supplementary Fig. 3d, e, and Videos 2, 3), which may reflect the ability of HIV to interfere with cytoskeletal processes involved in cell migration[15, 16].

While most infected LN cells resembled antigen-experienced T cell in terms of motility as well as size and shape, a subpopulation (10–20%) of cells stood out by their unusually elongated, thin, and sometimes branched trailing edges. These cells reached average skeletal lengths of at times more than 100 μm, while Tcm rarely exceeded 20 μm (Fig. 2g, h, Supplementary Videos 2–4). When we tracked skeletal lengths in individual cells along with their motility, we noted that some of the elongated cells continued to be motile (Fig. 2i). Similar results were obtained with SF162R3[17], a GFP-expressing strain derived from the primary R5-tropic clone SF162 (Supplementary Fig. 4 and Video 5).

Since it was possible that our flow cytometry analysis failed to detect these elongated cells (Fig. 2b), and that these were in fact not T cells, we wanted to determine unambiguously whether HIV-infected T cells could acquire such unusual morphological characteristics *in vivo*. Therefore, we adopted a co-culture method[18] to efficiently infect Tcm with HIV-GFP *in vitro* (Fig. 3a), and transferred these cells into footpads of BLT mice, from where they migrated to draining popLNs. Recipient BLT mice were pre-treated with a cocktail of antiviral drugs[6] to prevent infection of any host cells. Under these conditions, where the T cell identity of GFP^+ cells in popLNs was known, we observed the same overall reduction in motility as well as a sub-population of abnormally elongated cells at a similar frequency as after *in situ* infection (Fig. 3b–d **and** Supplementary Video 6). Co-injection of uninfected Tcm also confirmed that these and HIV-infected T cells localized to the same regions of the LN and that decreased motility of HIV-infected cells did not result from their sequestration into a particular microenvironment (Supplementary Fig. 5 and Video 6).

The elongated morphology could result from infection of a T cell population that has an intrinsic propensity to adopt such shapes. Alternatively, HIV proteins might actively induce this phenotype. To distinguish between these two possibilities, we generated a CCR5-using, HIV-derived lentiviral vector that expresses GFP, but no HIV proteins in infected cells (Fig. 3e). Two days after footpad injection, a similar number of GFP^+ cells were observed in draining LNs as after infection with HIV-GFP. However, these cells did not exhibit

elongated shapes. They also migrated faster than HIV-GFP-infected LN cells and at similar speeds as Tcm (Fig. 3f–h **and** Supplementary Video 7), further supporting that HIV induces migratory deceleration of infected cells. Thus, one or several HIV proteins induce the abnormal shapes and decreased motility of HIV-infected T cells.

During HIV assembly, which in migrating, polarized T cells takes place at the uropod[19], the HIV Env glycoprotein is exposed on the cell surface and can trigger the formation of intercellular adhesive contacts with CD4-expressing cells *in vitro*[20–23]. In the LN environment, where T cells are highly motile, such adhesive interactions could lead to abnormal uropod elongation through tethering of infected T cells to uninfected $CD4^+$ LN cells. Supporting this scenario, we consistently observed stationary behavior of the trailing edges of migrating T cells, often followed by their rapid retraction, perhaps reflecting sudden release of tethered uropods (Supplementary Video 8). Alternatively, cellular elongations could also result from the formation of multinucleated syncytia, which also depends on the function of Env[24]. In order to test if either uropod tethering or syncytia formation are involved in the elongation of HIV-infected T cells we generated HIV-GFP ΔEnv, where large parts of Env, including the CD4-binding region, are not expressed (Supplementary Fig. 6a). When *trans*-complemented with an exogenous R5 HIV envelope, the virus was as infectious as HIV-GFP, but no secondary infections occurred, as expected, since infected cells expressed no functional Env (Supplementary Fig. 6b–d). Strikingly, the elongated phenotype of infected LN cells was completely lost in absence of functional Env (Fig. 4a–c and Supplementary Video 9). However, cells infected with HIV-GFP ΔEnv still migrated at reduced speeds (Fig. 4b, c), suggesting that HIV factors other than Env were largely responsible for decreased T cell motility. Cell elongation did not result from artificial interactions of Env with murine adhesion or extracellular matrix proteins, since it was not observed in HIV-infected Tcm migrating in LNs of non-humanized mice (Fig. 4d **and** Supplementary Fig. 7). To test whether interactions of Env specifically with CD4, or with other human ligands, such as the $\alpha_4\beta_7$-integrin[25], are involved in tethering, we mutated HIV-GFP to exchange a single critical amino acid in Env (D368R in the HBX2 consensus sequence) to abrogate CD4-binding[26] (Supplementary Fig. 8). Cells infected with HIV-GFP D368R showed the same loss of cell elongation as observed after deletion of Env (Fig. 4d).

To examine if some of the highly elongated T cells are part of multinucleated syncytia, we analyzed infected BLT LNs by histology. However, while we did find GFP-expressing cells with multiple nuclei (not shown), we were unable to visualize the elaborate tethers observed by MP-IVM in thick tissue sections, which may explain in part why these presumably highly labile structures have not been observed in human histological tissue samples. Therefore, we generated HIV-nGFP, in which GFP is targeted to cell nuclei through addition of a nuclear localization signal (Supplementary Fig. 9). When we infected BLT mice with this strain, we observed by MP-IVM that the vast majority of elongated LN cells were multinucleated syncytia that, given the involvement of Env, most likely developed through cell fusion (Fig. 4e, f). These syncytia frequently migrated with their tightly clustered nuclei moving in a coordinated fashion, but intermittently dispersed so that individual nuclei moved in different directions, yet remained connected by long membrane tethers (Supplementary Video 10). However, both fused and unfused cells also formed free-ending tethers, indicating that those

were caused by adhesive interactions with non-visualized $CD4^+$ cells (Supplementary Video 11). While similar membrane tethers, such as nanotubes, can also form between T cells *in vitro* in the absence of viral infection[27], Env proteins of HIV and other retroviruses have been shown to facilitate their formation[23, 28]. Adhesive tethers may promote cell-to-cell viral transfer through VSs, or may reflect the initiation of cell fusion, or both.

Movement of free HIV virions within and between tissues is likely restricted by the limits of diffusion, by anatomical barriers, and by soluble immune factors, such as complement and natural antibody[2]. Allowing infected T cells to retain robust motility and to serve as migratory vehicles might therefore be a viral strategy for efficient local and systemic dissemination. If indeed long-range transport of HIV to distant tissues relies on the trafficking of infected cells during physiological T cell recirculation, then interfering with lymphocyte trafficking should limit systemic viral dissemination and reduce plasma viremia. To block T cell egress from LNs into efferent lymph vessels we treated BLT mice with the functional S1P receptor antagonist FTY720 (Fingolimod), which caused profound lymphopenia (Supplementary Fig. 10a).

Strikingly, in mice that received FTY720 starting at the time of infection with HIV-GFP, viral RNA in peripheral blood remained within or only slightly above background range (Fig. 4g), while the drug did not show antiviral activity in cell culture (Supplementary Fig. 10b). This result was confirmed with another R5-tropic strain, SF162R3 [17] (Fig. 4h). Two months after infection, viral RNA was strongly reduced, yet not absent from remote lymphoid tissues of treated animals (Supplementary Fig. 10c), suggesting that FTY720 in the longer term did not fully prevent, but only limited dissemination within the lymphoid system. Accordingly, development of viremia after withdrawal of FTY720 after 8 weeks of treatment indicated that the release of T cells from lymphoid tissues rapidly initiated efficient systemic viral replication (Fig. 4h). Interestingly, we also observed a reduction in viral load in the draining LN in long-term treated animals (Supplementary Fig. 10c). This may reflect local depletion of HIV T cell targets, but could also indicate that FTY720 treatment reduces viral replication through a general perturbation of T cell homeostasis or through delayed, direct antiviral activity, independently of its effect on the trafficking of HIV-infected T cells. However, FTY720 did not affect viremia in mice with pre-established infection (Fig. 4i), similar to what was observed in SHIV infection of macaques[29]. While we cannot rule out other direct or indirect effects of FTY720 on viral replication, the observation that HIV infection is limited and high-level viraemia prevented by interfering with T-cell recirculation before, but not after systemic viral dissemination, suggests an important role for the trafficking of infected, migratory T cells in the efficient transport of HIV from draining to remote lymphoid tissues.

In summary, we find that HIV induces a partial reduction in the motility of infected T cells, as well as their tethering to and fusion with $CD4^+$ immune cells in LNs. This may reflect the need for HIV to tune T cell migratory and interactive behavior in order to meet two opposing requirements: The use of motile cells as vehicles to disseminate within and between tissues, which inherently involves short-lived cell contacts; and the formation of VSs and, possibly, syncytia, for cell-to-cell spread, which likely requires longer-lasting cell contacts. Reduced motility of infected T cells might favor the formation and maintenance of

tethering contacts with potential HIV target cells, while still allowing for efficient trafficking to distant tissues.

METHODS SUMMARY

BLT humanized mice

Sublethally irradiated, female NOD/SCID mice were transplanted under the kidney capsule with 1mm^3 fragments of human fetal liver and thymus, and injected i.v. with 1–5 × 10^5 purified CD34$^+$ human fetal liver cells. After 18–20 weeks, healthy mice with >50% human lymphoid reconstitution in peripheral blood were used for experiments within 6 weeks. In experiments that did not require popliteal LNs, NOD/SCID x $\gamma c^{-/-}$ (NSG) mice were used as graft recipients.

HIV reporter strains

The CCR5-using, GFP-expressing virus NL4-3 IRES-GFP R5 ('HIV-GFP') was constructed from pBR-NL4-3-IRES-GFP-*nef*$^{+}$[12] by replacing the V3 loop region of *env* with the corresponding sequence from the R5 clone BaL. HIV-GFP ΔEnv and HIV-GFP D368R were generated by site-directed mutagenesis. To produce infectious HIV-GFP ΔEnv and HIV-GFP D368R, the BaL Env was *trans*-complemented using a helper plasmid during virus production. HIV-nGFP was generated by inserting the SV40 nuclear localization sequence N-terminal of GFP in HIV-GFP. The lentiviral vector pHAGE-CMV-GFP was packaged with the R5 Env and standard helper plasmids to produce the CCR5-using 'R5 LV-GFP', which expresses no HIV proteins in infected cells.

MP-IVM of HIV-infected cells in lymph nodes

For *in situ*-infection of LN cells, BLT mice were injected into the footpad with 0.5 – 1.5 × 10^5 infectious units of recombinant HIV or R5 LV-GFP. 48 hours later, the draining popLNs were imaged by MP-IVM, as described[4]. Alternatively, HIV-GFP-infected Tcm were injected into the footpads of BLT mice pretreated with antiretroviral drugs, and imaged by MP-IVM 12 hours later.

METHODS

BLT humanized mice

Female NOD/SCID (NS) and NOD/SCID x $\gamma_c^{-/-}$ (NSG) mice were purchased from Jackson Laboratories and reconstituted at age 6–8 weeks with human immune systems as previously described[30]. Briefly, mice were conditioned with sublethal (2 Gy) whole-body irradiation and transplanted with 1 mm^3 fragments of human fetal thymus and liver (17 to 19 weeks of gestational age, from Advanced Bioscience Resources) under the kidney capsule. CD34$^+$ cells were isolated from human fetal liver using anti-CD34 microbeads (Miltenyi Biotec) and injected intravenously (1 – 5 × 10^4 cells/mouse) within 6 hours of surgery to create "BLT" (*B*one marrow, *L*iver and *T*hymus) mice. Mice were monitored for human hematopoietic reconstitution at 14 and 18 weeks post-transplantation. High lymphoid reconstitution in peripheral blood (>25% lymphocytes in PBL, >50% human lymphocytes, >40% T cells among lymphocytes) correlated with optimal lymph node reconstitution

suitable for intravital imaging (typically at 18–20 weeks). NS mice were used for all experiments involving footpad injection of HIV or cells and analysis (e.g. by MP-IVM) of draining popliteal LNs. NSG mice, which lack popliteal, but possess cervical LNs, were used for long-term experiments involving FTY720 treatment.

OT-II TCR transgenic mice were obtained from Jackson Laboratories and bred in house. All experiments were performed in accordance to the rules and regulations of the Center of Comparative Medicine (CCM) and approved by the MGH Institutional Animal Care and Use Committee (IACUC) and the Harvard Medical Area Standing Committee on Animals.

Plasmids and virus production

The proviral plasmid pBR-NL43-IRES-EGFP-*nef*$^+$ (pIeG-*nef*$^+$)[31] was obtained from the NIH AIDS Research & Reference Reagent Program (ARRRP, Catalog #11349). The V3 loop of *env* was modified to resemble that of HIV BaL and confer R5-tropism, as previously described[32]. Briefly, a commercial kit (Stratagene) and primers 5′-cccaacaacaatacaagaaaaagtatacatataggaccaggcagagcattatat acaacaggagaaataataggagatataagacaagcacattgtaacattag-3′ and 5′-ctaatgttacaatgtgcttgtc ttatatctcctattatttctcctgttgtatataatgctctgcctggtcctatatgtatacttttttcttgtattgttgttggg-3′ were used according to the manufacturer's protocol to mutagenize pIeG-*nef*$^+$ and obtain pIeG-*nef*$^+$ R5. The non-GFP-expressing parental plasmid, pNL4-3, was similarly mutagenized to obtain pNL4-3 R5. Infectious virus generated form pIeG-*nef*+ R5 and pNL4-3 R5 are called 'HIV-GFP' and 'HIV' for short.

The pSVIIIexE7-ADA *env*-expressing vector (kindly provided by Dr. J. Sodroski) was modified by restriction cloning to express *env* from pIeG-*nef*$^+$ R5 using KpnI and BamHI restriction sites to obtain pSVIIIexE7-BaL.

To construct an *env*-deleted reporter construct, pIeG-*nef*$^+$ R5 was digested with PsiI (nucleotide 6865 and 7599) and re-ligated. The resulting frameshift mutation introduced a pre-mature stop codon while the RRE remained intact. The new plasmid pIeG-*nef*$^+$ Δ*env* was packaged with pSVIIIexE7-BaL to obtain HIV-GFP ΔEnv.

To construct the CD4-binding-deficient reporter virus HIV-GFP D368R, site-directed mutagenesis of pIeG-*nef*$^+$ R5 was performed using primers 5′-gcaatcctcaggagggcgcccagaaattgtaacg-3′ and 5′-cgttacaatttctgggcgccctcctgaggattgc-3′ (Stratagene). Successful mutagenesis was confirmed by DNA sequencing. HIV-GFP D368R was packaged with pSVIIIexE7-BaL to obtain single-round infectious viral supernatant.

The lentiviral vector construct pHAGE-CMV-GFP is a modification of a construct originally developed in the laboratory of Dr. Richard C. Mulligan at Harvard Medical School[33]. pHAGE-CMV-GFP was packaged with standard helper plasmids and pSVIIIexE7-BaL to obtain the non-replicating, R5-using vector R5 LV-GFP. To construct the vector pHAGE-NLS-Cerulean, first GFP was replaced in pHAGE-CMV-GFP with Cerulean using restriction enzyme sites NcoI and XmaI to obtain pHAGE-CMV-Cerulean. Then, the complementary primers 5′-agccccatggctccaaaaaagaagagaaaggtaggcgccatggct-3′ and 5′-agccatggcgcctacctttctcttctttttggagccatgggct-3′ were annealed, digested with NcoI and

inserted into pHAGE-CMV-Cerulean, placing the NLS peptide of SV40 immediately upstream of GFP. The same cloning strategy was used to construct HIV-nGFP from HIV-GFP.

Dr. Amanda Brown at Johns Hopkins University School of Medicine kindly provided pSF162R3.

All HIV and lentiviral stocks were produced by transfecting HEK293T cells using Lipofectamine 2000 (Invitrogen). Viral supernatants were clarified through a 0.22μm filter and centrifuged at 90,000 × g for 2 hours using an SW28Ti rotor (Beckman Coulter) over a 20% sucrose cushion. Viral stocks were titrated using MAGI.CCR5 cells and expressed as bfu/mL (blue focus units/mL) as described previously[34].

Cells

Human and murine $CD4^+$ T cells were purified from uninfected BLT and OT-II mice, respectively, by negative immuno-magnetic selection (Miltenyl Biotec), and labeled with 2 μM Celltracker green (CMFDA) or 10 μM Celltracker blue (CMAC, both from Invitrogen) before adoptive transfer into BLT mice (see below).

Human $CD4^+$ central memory-like T cells (Tcm) were generated as described previously with slight modifications[35]. Briefly, $CD4^+$ T cells were isolated from spleen and LNs of BLT mice by positive immuno-magnetic selection using CD4 microbeads (Miltenyi Biotec) to purities consistently above 95%. Cells were activated by adding Dynabeads coated with anti-human CD3ε/CD28 antibody (3:1 bead:cell ratio, Invitrogen) for 2 days in RPMI 1640 supplemented with 10% FCS (Atlanta Biologicals), 2 mM L-glutamine (Gibco), 1mM sodium pyruvate and 10mM HEPES (Mediatech). After 2 days, cells were washed and cultured for another 6–8 days in medium containing 50 IU/mL human rIL-2 (R&D Systems), keeping cell density close to 5×10^5 cells/mL. Cells were used for all experiments between days 8 and 10.

To infect Tcm with HIV-GFP with high efficiency, we used a modified co-culture method[36]. Briefly, 2×10^6 MAGI.CCR5 cells were transfected with 10μg of pIeG-*nef*$^+$ R5 and 24 hours later T cells were added to the confluent layer of virus-producing cells. Two days later, T cells were collected by Ficoll gradient centrifugation and washed three times before injection into BLT mice. Since with this approach we could only generate a limiting number of HIV-infected Tcm, we injected these into footpads for initially selective and efficient delivery to draining LNs,[37] since upon i.v. injection cells distributed to all secondary lymphoid tissue and accumulated in only smaller numbers in the popliteal LN under study. In some studies, HIV-infected Tcm were injected into the footpad of D_HLMP2a mice[38] depleted of NK cells through daily i.p. injections of 50μL anti-asialo GM1 antibody (Wako Chemicals Inc.) for 2 days.

To generate Tcm that were not infected with HIV-GFP, but expressed GFP for visualization by MP-IVM and comparison to HIV-GFP-infected cells, we transduced human T cells with VSV-G pseudotyped pHAGE-CMV-GFP on day 2 after activation. In some experiments,

uninfected Tcm were stained for 15 min at 37 C with 10 μM CellTracker Orange (CMTMR, Invitrogen) before footpad or i.v. injection into BLT mice.

MAGI.CCR5 (Cat. #3522), U87.CD4 (Cat. #4031), U87.CD4.CCR5 (Cat. #4035), U87.CD4.CXCR4 (Cat. #4036) cells were all obtained from the ARRRP.

T cell homing studies

Isogenic human and murine OT-II $CD4^+$ T cells were purified, differentially labeled with celltracker dyes, and injected i.v. into BLT mice. 18 hours later, flow cytometry was used to determine homing ratios based on the relative frequencies of human and mouse T cells injected and recovered in various tissues.

HIV infection of BLT mice

For analyses of HIV infection in popliteal LNs, BLT mice were injected into footpads with $5 \times 10^4 – 1.5 \times 10^5$ infectious units of various HIV strains.

For longer-term studies on the effects of FTY720 treatment on the course of infection, 4×10^4 infectious units of HIV-GFP were injected into the cheek skin of NSG-derived BLT mice, which is drained by cervical LNs.

Plasma viremia

Mice were bled from the superficial temporal vein at indicated times and sera stored at −80°C. Viral RNA was isolated from 20–70 μL of plasma using the QIAamp viral RNA kit (Qiagen), reverse transcribed, and cDNA amplified by qPCR using SYBR green (Qiagen) on the Lightcycler 480-II (Roche). Plasma from uninfected BLT mice was used to determine the RT-PCR background signal, which was consistently higher than the background signal obtained with water.

Quantitation of tissue viral load

Mice were sacrificed at the specified days and lymph nodes and spleen were removed and stored in 200μL of RNA*later* solution overnight (Ambion). Single-cell suspensions from tissues were obtained using the gentle MACS dissociator (Miltenyi Biotec) and RNA was extracted using a commercial kit (Qiagen). Quantification of viral RNA was performed as described above. Viral loads were normalized to total tissue RNA.

Pharmacological treatments

1 mg/kg BW FTY720 or vehicle was injected i.p every other day starting 1 hour before HIV infection of BLT mice to block T cell egress from LNs.[39]

100 mg/kg emtricitabine (FTC) and 150 mg/kg tenofovir disoproxil fumarate (TDF) were i.p. injected daily starting 2 days before footpad injection of HIV-infected Tcm to prevent infection of recipient BLT mice.

Intravital multiphoton microscopy and image analysis

BLT mice were anaesthetized and the popLNs microsurgically exposed for MP-IVM as previously described[40]. Imaging depth was typically 80–200 μm below the LN capsule. For multiphoton excitation and second harmonic generation, a MaiTai Ti:sapphire laser (Newport/Spectra-Physics) was tuned to between 830 and 920 nm for optimized excitation of the fluorescent probes used. For four-dimensional recordings of cell migration, stacks of 11 optical sections (512 × 512 pixels) with 4–5 μm z-spacing were acquired every 15 or 24 seconds to provide imaging volumes of 40 μm in depth. Emitted light and second harmonic signals were detected through 455/50 nm, 525/50 nm, 590/50 nm, and 665/65 band-pass filters with non-descanned detectors.

Data sets were transformed in Imaris 7.3.1 (Bitplane) to generate maximum intensity projections (MIPs) for export as Quicktime movies. Since automated 3D-tracking of cell migration through Imaris did not perform well on the complex shapes of elongated HIV-infected cells, we used automated or manual 2D-tracking of cell centroids for all motility analyses, which yielded slightly lower velocity measurements than 3D-tracking. 2D-cell lengths were measured in ImageJ as the longest path connecting front and end of unbranched cells or as the sum of path lengths of all branches of individual branched cells (“cell skeletal length”). Either instantaneous (frame-by-frame) cell lengths or average cell lengths for individual cell tracks are provided. Cell step and track parameters were further analyzed in Matlab (Mathworks).

All time-lapse sequences are accelerated 360x over real-time for display as Quicktime movies.

Flow cytometry

Phenotypic characterization of T cells was performed on an LSRII (Becton Dickinson), using FlowJo software (Tree Star) for analysis. Spleen and LNs were minced with fine forceps and passed through a 40 μm mesh to obtain single cell suspensions. Cells were washed, counted and stained with a panel of directly conjugated anti-human mAbs: CD3-APC/Cy7 (HIT3a), CD4-PE/Cy7 (OKT4), CCR7-APC (TG8), CD8-PerCP (RPA-T8), CD45RA-PE (HI100), CD45RO-PE (UCHL1), MHC-I-PerCP (W6/32), CCR5-PE (HEK/1/85a) and CD62L-Alexa488 (DREG-56) (Biolegend).

HIV-infected cells were fixed with 2% PFA after staining before analysis.

Immunohistochemistry

Frozen sections of BLT and C57BL/6 LNs previously fixed in paraformaldehyde were processed for histological analysis using standard techniques. Briefly, 20 μm frozen sections were permeabilized with Triton X-100, blocked with BSA and anti-CD16/32, and stained with polyclonal anti-desmin rabbit IgG (ab15200; abcam) and either mouse anti-human CD4 mouse IgG1 (clone RPA-T4, Biolegend) or FITC-anti-murine CD4 rat IgG2b (clone GK1.5, Biolegend) antibodies. Alexa Fluor 555-anti-rabbit IgG (A31572, Invitrogen) and FITC-anti mouse IgG (ab97022, Abcam) were used as secondary antibodies. Stained sections were

embedded in VectaShield Hard set (Vector H-1400) and analyzed by multiphoton microscopy.

Statistical analysis

Unpaired Student's *t*-test and Mann-Whitney U test were used for comparisons of data sets with normal or non-normal distribution, respectively, using Prism 5 (GraphPad). For the homing studies, one-sample t test was used for comparison to a hypothetical value of 1, corresponding to identical homing efficiency. When p-values were smaller than 0.05, differences were considered as significant.

Supplementary Material

Refer to Web version on PubMed Central for supplementary material.

Acknowledgments

We thank Dr. J. Sodroski for the pSVIIIexE7 plasmid and Dr. A. Brown for $HIV_{SF162R3}$; Drs. H.S. Shin as well as T. Tivey, K. Bankert and S. Tanno for technical assistance with the generation of humanized mice; Drs. A. Peixoto and D. Alvarez for management of the $BL2^{+}$ multiphoton microscopy facility; Drs. A. Brass, T. Allen and T. Dudek at the Ragon Institute for assistance with virological techniques; and Mrs. N. Elpek, M. Byrne and A. Finzi for technical assistance. Funding for this study was through NIH grants P01 AI0178897, R56 AI097052, R01 CA150975, P30 AI060354, and a Platform Award from the Ragon Institute of MGH, MIT and Harvard. T.T.M. was supported by the MGH ECOR Tosteson Postdoctoral Fellowship Award and the NIH training grant T32 AI007387.

References

1. Haase AT. Early events in sexual transmission of HIV and SIV and opportunities for interventions. Annu Rev Med. 2011; 62:127–39. [PubMed: 21054171]
2. Sattentau Q. Avoiding the void: cell-to-cell spread of human viruses. Nat Rev Microbiol. 2008; 6:815–26. [PubMed: 18923409]
3. Gebhardt T, et al. Different patterns of peripheral migration by memory CD4+ and CD8+ T cells. Nature. 2011; 477:216–9. [PubMed: 21841802]
4. Mempel TR, Henrickson SE, von Andrian UH. T-cell priming by dendritic cells in lymph nodes occurs in three distinct phases. Nature. 2004; 427:154–9. [PubMed: 14712275]
5. Melkus MW, et al. Humanized mice mount specific adaptive and innate immune responses to EBV and TSST-1. Nat Med. 2006; 12:1316–22. [PubMed: 17057712]
6. Denton PW, et al. Antiretroviral pre-exposure prophylaxis prevents vaginal transmission of HIV-1 in humanized BLT mice. PLoS Med. 2008; 5:e16. [PubMed: 18198941]
7. Sun Z, et al. Intrarectal transmission, systemic infection, and CD4+ T cell depletion in humanized mice infected with HIV-1. J Exp Med. 2007; 204:705–14. [PubMed: 17389241]
8. Brainard DM, et al. Induction of robust cellular and humoral virus-specific adaptive immune responses in human immunodeficiency virus-infected humanized BLT mice. J Virol. 2009; 83:7305–21. [PubMed: 19420076]
9. von Andrian UH, Mempel TR. Homing and cellular traffic in lymph nodes. Nature Reviews Immunology. 2003; 3:867–878.
10. Worbs T, Mempel TR, Bolter J, von Andrian UH, Forster R. CCR7 ligands stimulate the intranodal motility of T lymphocytes in vivo. J Exp Med. 2007; 204:489–95. [PubMed: 17325198]
11. Bajenoff M, et al. Stromal Cell Networks Regulate Lymphocyte Entry, Migration, and Territoriality in Lymph Nodes. Immunity. 2006; 25:989–1001. [PubMed: 17112751]

12. Schindler M, Munch J, Kirchhoff F. Human immunodeficiency virus type 1 inhibits DNA damage-triggered apoptosis by a Nef-independent mechanism. J Virol. 2005; 79:5489–98. [PubMed: 15827163]
13. Chen BK, Gandhi RT, Baltimore D. CD4 down-modulation during infection of human T cells with human immunodeficiency virus type 1 involves independent activities of vpu, env, and nef. J Virol. 1996; 70:6044–53. [PubMed: 8709227]
14. Zhang Z, et al. Sexual transmission and propagation of SIV and HIV in resting and activated CD4+ T cells. Science. 1999; 286:1353–7. [PubMed: 10558989]
15. Stolp B, et al. HIV-1 Nef interferes with host cell motility by deregulation of Cofilin. Cell Host Microbe. 2009; 6:174–86. [PubMed: 19683683]
16. Nobile C, et al. HIV-1 Nef inhibits ruffles, induces filopodia, and modulates migration of infected lymphocytes. J Virol. 2010; 84:2282–93. [PubMed: 20015995]
17. Brown A, Gartner S, Kawano T, Benoit N, Cheng-Mayer C. HLA-A2 down-regulation on primary human macrophages infected with an M-tropic EGFP-tagged HIV-1 reporter virus. J Leukoc Biol. 2005; 78:675–85. [PubMed: 16000390]
18. Casartelli N, et al. Tetherin restricts productive HIV-1 cell-to-cell transmission. PLoS Pathog. 2010; 6:e1000955. [PubMed: 20585562]
19. Llewellyn GN, Hogue IB, Grover JR, Ono A. Nucleocapsid promotes localization of HIV-1 gag to uropods that participate in virological synapses between T cells. PLoS Pathog. 2010; 6:e1001167. [PubMed: 21060818]
20. Jolly C, Kashefi K, Hollinshead M, Sattentau QJ. HIV-1 cell to cell transfer across an Env-induced, actin-dependent synapse. J Exp Med. 2004; 199:283–93. [PubMed: 14734528]
21. Chen P, Hubner W, Spinelli MA, Chen BK. Predominant mode of human immunodeficiency virus transfer between T cells is mediated by sustained Env-dependent neutralization-resistant virological synapses. J Virol. 2007; 81:12582–95. [PubMed: 17728240]
22. Hubner W, et al. Quantitative 3D video microscopy of HIV transfer across T cell virological synapses. Science. 2009; 323:1743–7. [PubMed: 19325119]
23. Rudnicka D, et al. Simultaneous cell-to-cell transmission of human immunodeficiency virus to multiple targets through polysynapses. J Virol. 2009; 83:6234–46. [PubMed: 19369333]
24. Sodroski J, Goh WC, Rosen C, Campbell K, Haseltine WA. Role of the HTLV-III/LAV envelope in syncytium formation and cytopathicity. Nature. 1986; 322:470–4. [PubMed: 3016552]
25. Arthos J, et al. HIV-1 envelope protein binds to and signals through integrin alpha4beta7, the gut mucosal homing receptor for peripheral T cells. Nat Immunol. 2008; 9:301–9. [PubMed: 18264102]
26. Thali M, et al. Effects of changes in gp120-CD4 binding affinity on human immunodeficiency virus type 1 envelope glycoprotein function and soluble CD4 sensitivity. J Virol. 1991; 65:5007–12. [PubMed: 1870209]
27. Sowinski S, et al. Membrane nanotubes physically connect T cells over long distances presenting a novel route for HIV-1 transmission. Nat Cell Biol. 2008; 10:211–9. [PubMed: 18193035]
28. Sherer NM, et al. Retroviruses can establish filopodial bridges for efficient cell- to-cell transmission. Nat Cell Biol. 2007; 9:310–5. [PubMed: 17293854]
29. Kersh EN, et al. Evaluation of the lymphocyte trafficking drug FTY720 in SHIVSF162P3-infected rhesus macaques. J Antimicrob Chemother. 2009; 63:758–62. [PubMed: 19218272]
30. Brainard DM, et al. Induction of robust cellular and humoral virus-specific adaptive immune responses in human immunodeficiency virus-infected humanized BLT mice. Journal of Virology. 2009; 83:7305–21. [PubMed: 19420076]
31. Schindler M, et al. Down-modulation of mature major histocompatibility complex class II and up-regulation of invariant chain cell surface expression are well-conserved functions of human and simian immunodeficiency virus nef alleles. J Virol. 2003; 77:10548–56. [PubMed: 12970439]
32. Hwang SS, Boyle TJ, Lyerly HK, Cullen BR. Identification of the envelope V3 loop as the primary determinant of cell tropism in HIV-1. Science. 1991; 253:71–4. [PubMed: 1905842]
33. Mostoslavsky G, Fabian AJ, Rooney S, Alt FW, Mulligan RC. Complete correction of murine Artemis immunodeficiency by lentiviral vector- mediated gene transfer. Proc Natl Acad Sci U S A. 2006; 103:16406–11. [PubMed: 17062750]

34. Pirounaki M, Heyden NA, Arens M, Ratner L. Rapid phenotypic drug susceptibility assay for HIV-1 with a CCR5 expressing indicator cell line. J Virol Methods. 2000; 85:151–61. [PubMed: 10716348]
35. Bondanza A, et al. Suicide gene therapy of graft-versus-host disease induced by central memory human T lymphocytes. Blood. 2006; 107:1828–36. [PubMed: 16293601]
36. Casartelli N, et al. Tetherin restricts productive HIV-1 cell-to-cell transmission. PLoS Pathog. 2010; 6:e1000955. [PubMed: 20585562]
37. Debes GF, et al. Chemokine receptor CCR7 required for T lymphocyte exit from peripheral tissues. Nat Immunol. 2005; 6:889–94. [PubMed: 16116468]
38. Casola S, et al. B cell receptor signal strength determines B cell fate. Nat Immunol. 2004; 5:317–27. [PubMed: 14758357]
39. Schwab SR, Cyster JG. Finding a way out: lymphocyte egress from lymphoid organs. Nat Immunol. 2007; 8:1295–301. [PubMed: 18026082]
40. Murooka TT, Mempel TR. Multiphoton intravital microscopy to study lymphocyte motility in lymph nodes. Methods Mol Biol. 2012; 757:247–57. [PubMed: 21909917]

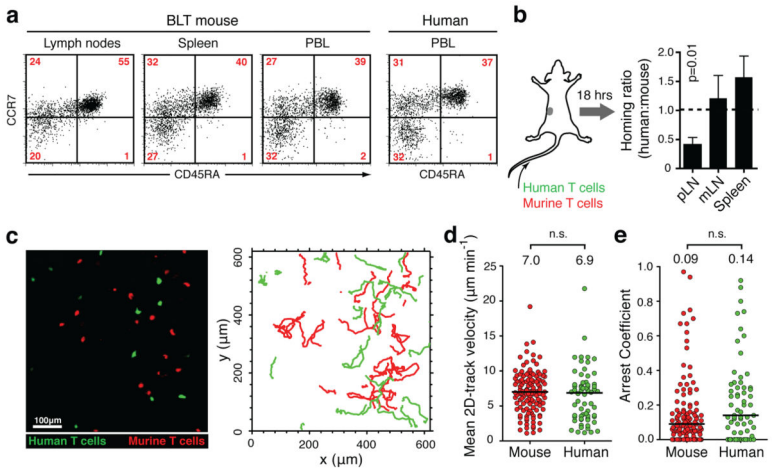

FIGURE 1. Human T cell migration in lymph nodes of BLT mice

a. Human CD4^{+}T cells with naïve (CD45RA^{+} CCR7^{+}), central memory (CD45RA^{-}, CCR7^{+}) and effector memory (CD45RA^{-}, CCR7^{-}) phenotype are represented in lymphoid organs and peripheral blood of BLT mice. Relative frequencies in blood are similar to humans. Plots are gated on hCD4^{+}, hCD3^{+} cells. **b.** Homing of human and murine CD4^{+} T cells into lymphoid tissues (pLN=peripheral, mLN=mesenteric LNs). Data pooled from three independent experiments. Values are means±s.e.m. **c.** Multiphoton intravital micrograph of a BLT popliteal LN 24 hours after adoptive transfer of human (green) and murine (red) T cells. Graph on the right shows migratory tracks of each population during a 30-minute recording. **d, e.** Mean 2D-track velocities (d) and arrest coefficients (e) of murine and human T cells in BLT LNs. Lines and numbers indicate medians. Data pooled from three recordings/two independent experiments.

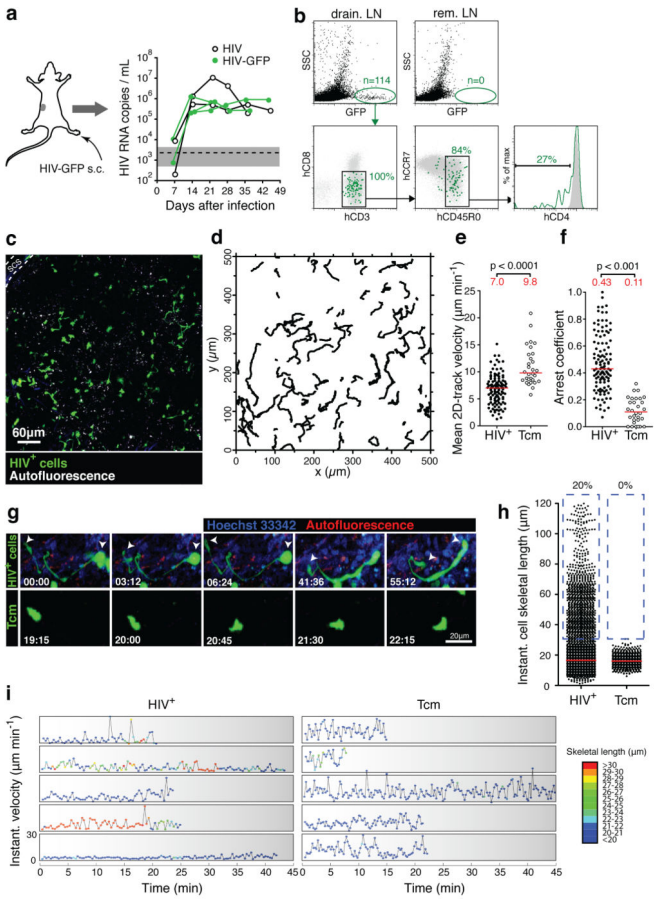

FIGURE 2. ***In vivo*** **dynamics and phenotype of HIV-infected LN cells**

a. Footpad injection of BLT mice with HIV-GFP produces robust and sustained viremia. 'HIV' is identical to HIV-GFP but lacks an IRES-GFP cassette. Similar results as shown here for 5 mice were obtained with other routes of infection (Supplementary Fig. 2d). Dashed line and grey-shaded area indicate mean and 95% confidence interval of background signals obtained from plasma of uninfected mice. **b.** Draining and non-draining LN cells two days after footpad infection with HIV-GFP. Grey dot plots and histograms show $GFP^{-}SSC^{low}$ LN cells. rem. LN: remote LNs. **c.** An intravital micrograph recorded from a popLN two days after footpad infection with HIV-GFP. **d.** Migratory tracks of GFP^{+} LN cells during a 30-minute recording. **e, f.** Mean 2D-track velocities (e) and arrest coefficients (f) of HIV^{+} LN cells compared to uninfected, GFP-expressing Tcm, recorded in LNs of uninfected BLT mice. Lines and numbers indicate medians. Data on HIV-infected LN cells and Tcm are representative of four and two independent experiments, resp. **g**. MP-IVM time-lapse recordings of an HIV-infected LN cell (top) and an uninfected Tcm (bottom) in BLT LNs. Arrows indicate leading and trailing edge of the infected cell. Elapsed time in min:sec. **h.** Instantaneous cell skeletal length of HIV-infected LN cells and Tcm from recordings as shown in (g). Lines indicate medians. Percentages indicate events>30 µm, highlighted by dashed blue box. **i.** Representative traces of infected LN cells and Tcm showing instantaneous cell skeletal length (color-coded) and instantaneous migratory

velocity over time. Traces selected from 142 recorded in 4 movies/3 independent experiments.

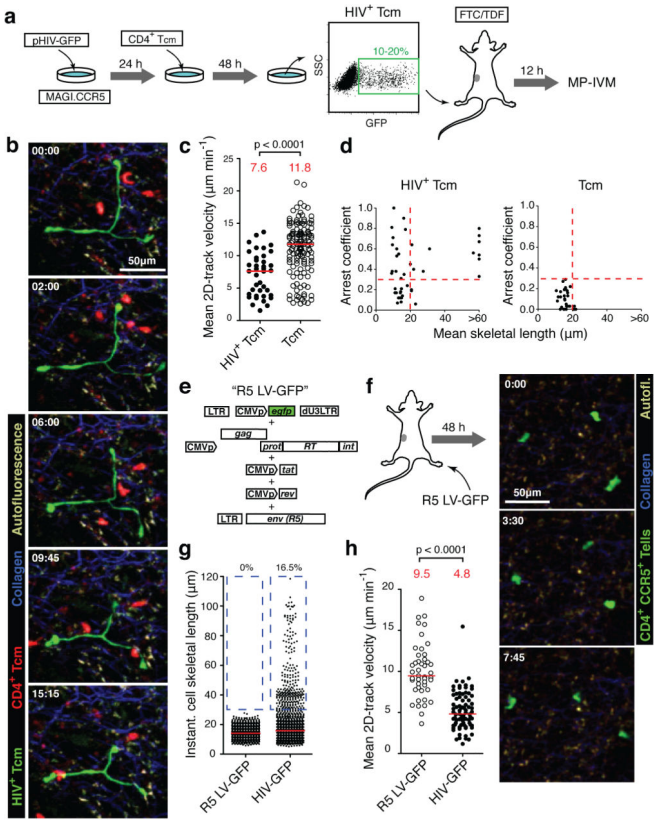

FIGURE 3. HIV induces an elongated phenotype in infected T cells

a. Analysis of *in vitro* HIV-infected Tcm in BLT LNs. FTC: Emtricitabine; TDF: Tenofovir. **b**. MP-IVM time-lapse series of uninfected (red) and HIV$^+$ (green) Tcm in a BLT LN. Elapsed time in min:sec. **c.** Mean 2D-track velocities. Red lines and numbers indicate medians. **d.** Correlation of mean cell skeletal length and arrest coefficient of individual cells. Dashed lines indicate threshold values based on measurements of uninfected Tcm. Data pooled from two independent experiments. **e.** Production of an R5-tropic, GFP-expressing lentiviral vector. **f.** 48 hours after footpad injection of 1.4×10^5 infectious units, GFP$^+$ cells are found in draining LNs. **g, h**. These cells do not elongate (g) and do not show the reduction of cell motility of HIV-infected LN cells (h). Percentages in (g) refer to cells >30 μm, highlighted by dashed blue box. The red lines and numbers in (h) indicate medians. Data are representative of two independent experiments/three mice.

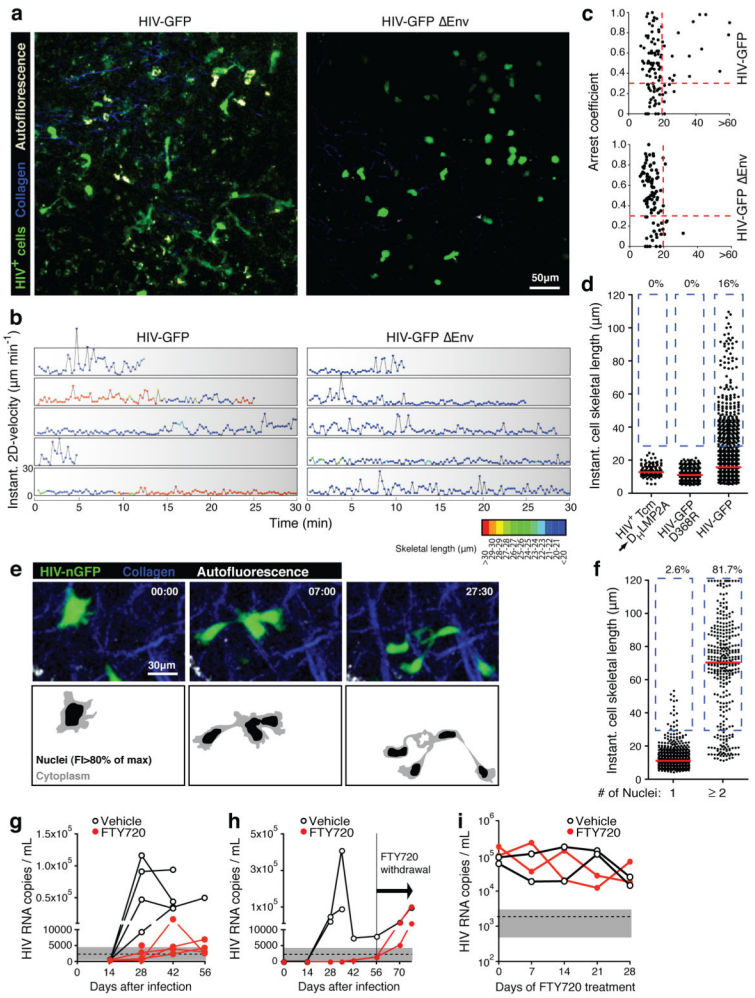

FIGURE 4. HIV-infected T cells tether to other LN cells and form syncytia through Env, and migrate to distant tissues to disseminate infection

a. Intravital micrographs from LNs of BLT mice injected 48 hours earlier with HIV-GFP (left) in one, and HIV-GFP ΔEnv (right) into the other footpad. **b.** Representative traces of infected T cells depicting instantaneous cell skeletal length (color-coded) and migratory velocity over time. Traces selected from 281 recorded in 14 movies/3 independent experiments. **c.** Mean cell skeletal length and arrest coefficient of individual cells infected with HIV-GFP or HIV-GFP ΔEnv. Data are pooled from six and eight recordings, respectively, from three independent experiments. **d.** Cell lengths of HIV-GFP-infected Tcm injected into NK cell-depleted, antibody-deficient D_HLMP2A mice, and of BLT LN cells infected *in situ* with HIV-GFP D368R or HIV-GFP. **e.** Recording of LN cells infected with HIV-nGFP. Bottom panels indicate border between cytoplasm and nuclei, based on a 80% of maximum fluorescence intensity (FI) threshold. **f.** Cell lengths of mono- and multinucleated, HIV-infected cells. **g, h.** Viremia in NSG BLT mice treated with FTY720 or vehicle starting at the day of s.c. HIV-infection via the cheek skin. **g**. Infection with HIV-GFP. **h**. Infection with clone SF162R3. FTY720 treatment was ended at day 56. **i**. Plasma

viremia under FTY-treatment started four weeks after in i.p-infection, when virema had stabilized. One representative experiment of two is shown.